[(Cp*)(dppe)Fe(III)−]$^+$ Units Bridged through 1,3-Diethynylbenzene and 1,3,5-Triethynylbenzene Spacers: Ferromagnetic Metal−Metal Exchange Interaction

Tania Weyland,[†] Karine Costuas,[‡] Alain Mari,[§] Jean-François Halet,*[,‡] and Claude Lapinte*[,†]

Organométalliques et Catalyse, UMR CNRS 6509, and Laboratoire de Chimie du Solide et Inorganique Moléculaire, UMR CNRS 6511, Université de Rennes 1, 35042 Rennes Cedex, France, and Laboratoire de Chimie de Coordination du CNRS, 205 Route de Narbonne, 31077 Toulouse Cedex, France

Received September 17, 1998

The bi- and trinuclear iron(III) complexes [1,3-{Cp*(dppe)Fe(C≡C−)}$_2$(C$_6$H$_4$)][PF$_6$]$_2$ (**2**$^{2+}$) and [1,3,5-{Cp*(dppe)Fe(C≡C−)}$_3$(C$_6$H$_3$)] [PF$_6$] (**3**$^{3+}$) were prepared by oxidation of [1,3-{Cp*-(dppe)Fe(C≡C−)}$_2$(C$_6$H$_4$)] or [1,3,5-{Cp*(dppe)Fe(C≡C−)}$_3$(C$_6$H$_3$)] with 2 or 3 equiv of [(C$_5$H$_5$)$_2$Fe][PF$_6$], respectively. Complexes **2**$^{2+}$ and **3**$^{3+}$ were isolated as thermally and air stable blue microcrystalline solids in 95 and 80% yield, respectively. These paramagnetic compounds were characterized by cyclic voltammetry, IR, UV−vis, ^{1}H NMR, Mössbauer, and ESR spectroscopies. The three organoiron groups of **3**$^{3+}$ are not located on the same side of the molecule, and its two faces are therefore magnetically nonequivalent. The ^{1}H NMR isotropic shifts are expected to be essentially contact shifts and the zfs (zero field splitting) parameter D is expected to be small for **2**$^{2+}$ and **3**$^{3+}$ since the Curie law is accurately obeyed for the proton resonances of the π-bound Cp* ligand. ESR spectra of the bi- and triradicals showed broad and unresolved signals at $g = 2.10$ (**2**$^{2+}$, $\Delta H_{pp} = 550$ G) and 2.13 (**3**$^{3+}$, $\Delta H_{pp} = 170$ G) in addition to signals at $g = 4.55$ and 4.46, respectively due to $\Delta m_s = 2$ transition. The $\Delta m_s = 3$ transition was observed at $g = 7.97$ in the spectrum of **3**$^{3+}$. The temperature dependence of molar susceptibility obtained by SQUID measurements on microcrystalline samples suggested that the ferromagnetic interaction produces a triplet ground state in biradical **2**$^{2+}$ ($2J = 130.6 \pm 0.2$ cm^{-1}) and a quartet ground state for triradical **3**$^{3+}$. The two doublet states lie above the quartet by 18.7 ± 0.2 and 28.8 ± 0.2 cm^{-1}. These results constitute the first examples of magnetic exchange interactions in a three-spin organometallic system with a triangular topology and the ferromagnetic coupling occurs at nanoscale distances between the metal spin carriers. The geometries of **2**$^{2+}$ and **3**$^{3+}$ were optimized using DFT calculations. High spin species were computed to be energetically favored with the spin density mainly localized on the iron centers supporting the experimental results.

Introduction

In the design of high-spin organic molecules, the *m*-phenylene framework has been recognized as the most reliable ferromagnetic coupling unit. Typical examples illustrating this strategy are super-high-spin polycarbenes,[1−7] poly(triphenylmethyl)s,[8−17] and stable high-spin poly(*N*-*tert*-butyl nitroxide)s.[18,19] The origin of the ferromagnetic coupling of spin-containing structures connected through *m*-phenylene spacers was expressed in terms of molecular topology for this alternant π-system and is known as the Ovchinnikov rule.[20−22] According to this rule, the carbon atoms of the alternant

[†] Organométalliques et Catalyse, Université de Rennes.
[‡] Laboratoire de Chimie du Solide et Inorganique Moléculaire, Université de Rennes.
[§] Laboratoire de Chimie de Coordination du CNRS.

(1) Iwamura, H.; Matsuda, K. In *Modern Acetylene Chemistry*; Stang, P. J., Diederich, F., Eds.; VCH: Weinheim, 1995; Chapter 11.
(2) Teki, Y.; Takui, T.; Itoh, K.; Kobayashi, K. *J. Am. Chem. Soc.* **1986**, *108*, 2147−2156.
(3) Izuoka, A.; Murata, S.; Sugawara, T.; Iwamura, H. *J. Am. Chem. Soc.* **1987**, *109*, 2631−2639. Fujita, I.; Teki, Y.; Takui, T.; Kinoshita, T.; Itoh, K.; Miko, F.; Sawaki, Y.; Iwamura, H.; Izuoka, A.; Sugawara, T. *J. Am. Chem. Soc.* **1990**, *112*, 4074−4075.
(4) Nakamura, N.; Inoue, K.; Iwamura, H.; Fujioka, T.; Sawaki, Y. *J. Am. Chem. Soc.* **1992**, *114*, 1484−1485.
(5) Matsuda, K.; Nakamura, N.; Takahashi, K.; Inoue, K.; Koga, N.; Iwamura, H. *J. Am. Chem. Soc.* **1995**, *117*, 5550−5560.
(6) Nakamura, N.; Inoue, K.; Iwamura, H. *Angew. Chem., Int. Ed. Engl.* **1993**, *32*, 872−874.
(7) Matsuda, K.; Nakamura, N.; Inoue, K.; Koga, N.; Iwamura, H. *Chem. Eur. J.* **1996**, *2*, 259−264.
(8) Veciana, J.; Rovira, C.; Crespo, M. I.; Armet, O.; Domingo, V.; Palacio, F. *J. Am. Chem. Soc.* **1991**, *113*, 2552−2561.
(9) Veciana, J.; Rovira, C.; Ventosa, N.; Crespo, M. I.; Palacio, F. *J. Am. Chem. Soc.* **1993**, *115*, 57−64.
(10) Rajca, A.; Utamapanya, S.; Xu, J. *J. Am. Chem. Soc.* **1991**, *113* (3), 9235−9241.
(11) Rajca, A. *J. Am. Chem. Soc.* **1990**, *112*, 5889−5892.
(12) Rajca, A.; Utamapanya, S.; Thayumanavan, S. *J. Am. Chem. Soc.* **1992**, *114*, 1884−1885.
(13) Rajca, A.; Utamapanya, S. *J. Am. Chem. Soc.* **1993**, *115*, 2396−2401.
(14) Rajca, A.; Rajca, S.; Padmakumar, R. *Angew. Chem., Int. Ed. Engl.* **1994**, *33*, 2091−2092.
(15) Rajca, A.; Rajca, S.; Desai, S. R. *J. Am. Chem. Soc.* **1995**, *117*, 806−816.
(16) Rajca, A.; Rajca, S. *J. Am. Chem. Soc.* **1996**, *118*, 8121−8126.
(17) Rajca, S.; Rajca, A. *J. Am. Chem. Soc.* **1995**, *117*, 9172−9179.

10.1021/om980778h CCC: $15.00
Publication on Web 11/13/1998

Scheme 1

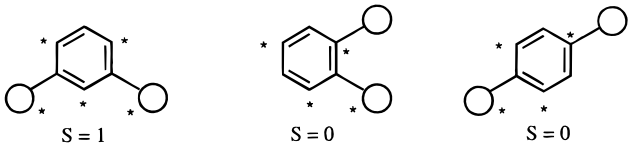

π-system of neutral biradicals can be divided in two sets, "*" and "non-*", such that no two members of the same set are connected. If the "*" set outnumbers the "non-*" by 2, a triplet ground state is expected and the spin density will reside only on the starred atoms, otherwise the singlet is the ground state (Scheme 1). As depicted in Scheme 1, the *meta* connection of the $S = 1/2$ spin carriers through a phenyl ring should give rise to a triplet ground state ($S = 1$), whereas a singlet ground state ($S = 0$) is expected from the *ortho* or *para* connections.

The general character of this rule has been strongly established for organic spin carriers, but formal violations of the rule were reported in particular cases.[23,24] The approaches based on this concept were very productive for the development of purely organic ferromagnets,[25,26] and the possibility of designing ferromagnetic polymers by this way was also recognized many years ago.[27]

The use of organometallic building blocks in the design of molecular-based magnets has received less attention despite the fact that the first molecular magnet described in 1986 was an organometallic compound.[28−30] The ability of many transition metal complexes to be stable in different oxidation states should be an advantage in the design of molecular magnetic materials compared to purely organic molecules. This is particularly interesting in the case of two or more robust organometallic building blocks with 18 or 17 valence electrons incorporated in different sites of the molecule. The magnetic properties of the molecule could then be triggered by changing the metal oxidation state upon electron-transfer processes. Moreover, it has not been established whether the Ovchinnikov topological rule will hold if transition metal spin carriers are connected with *m*-phenylene spacers. The question of the triplet ground state is specially interesting in the case of metal-centered spin carriers.

On the other hand, a third spin carrier can be placed at equal distances from the two others, providing discrete molecular species in which the nature of the interaction between adjacent centers is rigorously the same as in the biradical compounds, but the presence of a third spin carrier may lead to new magnetic behaviors as shown in Scheme 2.[26] Numerous pure inorganic or organic compounds with this triangular geometry have been described, whereas the use of organometallic building blocks remains an almost unknown area.[31] Moreover, for most of these triradicals the distances between the atoms where the spin density resides are short, significantly below the nanoscale limit (10 Å).

Scheme 2

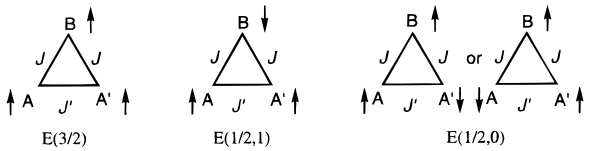

Scheme 3

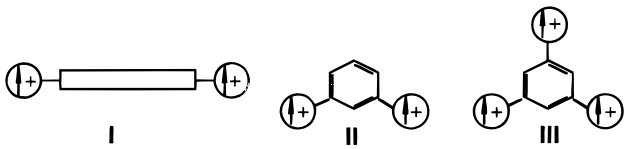

Our group is involved in both the synthesis and the study of the very special coupling properties of elemental carbon chains bridging two iron centers (Scheme 3 **I**) and in the construction of molecular assemblies containing several organometallic building blocks covalently connected through an all-π-delocalized organic spacer with a precisely controlled geometry.[32−34] The study of the mutual influence between the metal centers of a two-dimensional molecule in which two or three electron-rich organometallic building blocks are spanned by a poly(ethynyl)aryl ligand has been the target of a recent work (Scheme 3, **II** and **III**).[35] In these molecular devices the metal−metal interactions are rather strong in comparison with the similar systems recently reported.[36−38]

We describe here the first examples of organometallic molecules with two- and three-metal-centered spin carriers connected through a spacer with a rigid *m*-phenylene framework. The 17-electron low-spin iron(III) Cp*(dppe)Fe building blocks, which provide very stable organometallic radicals ($S = 1/2$), were linked to the connecting arene using an ethynyl fragment. It was previously established that this arrangement provides nanoscopic molecular devices with iron−iron intramolecular distances significantly longer than the intermo-

(18) Ishida, T.; Iwamura, H. *J. Am. Chem. Soc.* **1991**, *113*, 4238−4241.
(19) Kanno, F.; Inoue, K.; Koga, N.; Iwamura, H. *J. Phys. Chem.* **1993**, *97*, 13267−13283.
(20) Borden, W. T.; Davidson, E. R. *J. Am. Chem. Soc.* **1977**, *99*, 4587−4594.
(21) Ovchinnikov, A. *Theor. Chim. Acta* **1978**, *47*, 297−304.
(22) West, A. P.; Silverman, S. K.; Dougherty, D. A. *J. Am. Chem. Soc.* **1996**, *118*, 1452−1463.
(23) Kanno, F.; Inoue, K.; Koga, N.; Iwamura, H. *J. Am. Chem. Soc.* **1993**, *115*, 847−850.
(24) Fujita, J.; Tanaka, M.; Suemune, H.; Koga, N.; Matsuda, K.; Iwamura, H. *J. Am. Chem. Soc.* **1996**, *118*, 9347−9351.
(25) Iwamura, H. *Adv. Phys. Org. Chem.* **1990**, *26*, 179.
(26) Kahn, O. *Molecular Magnetism*; VCH Publishers: New York, 1993.
(27) Mataga, N. *Theor. Chim. Acta* **1968**, *10*, 372.
(28) Miller, J. S.; Calabrese, J. C.; Epstein, A. J.; Bigelow, R. W.; Zhang, J. H.; Reiff, W. M. *J. Chem. Soc., Chem. Commun.* **1986**, 1026−1028.
(29) Miller, J. S.; Epstein, A. J.; Reiff, W. M. *Chem. Rev.* **1988**, *88*, 201−220.
(30) Pei, Y.; Verdaguer, M.; Kahn, O.; Sletten, J.; Renard, J. P. *J. Am. Chem. Soc.* **1986**, *108*, 7428.
(31) Beck, W.; Niemer, B.; Wieser, M. *Angew. Chem., Int. Ed. Engl.* **1993**, *32*, 923−949.
(32) Le Narvor, N.; Lapinte, C. *Organometallics* **1995**, *14*, 634−639.
(33) Le Narvor, N.; Toupet, L.; Lapinte, C. *J. Am. Chem. Soc.* **1995**, *117*, 7129−7138.
(34) Coat, F.; Lapinte, C. *Organometallics* **1996**, *15*, 477−480. Guillemot, M.; Toupet, L.; Lapinte, C. *Organometallics* **1998**, *1928*, 8−1930.
(35) Weyland, T.; Lapinte, C.; Frapper, G.; Calhorda, M. J.; Halet, J.-F.; Toupet, L. *Organometallics* **1997**, *16*, 2024−2031.
(36) Fink, H.; Long, N. J.; Martin, A. J.; Opromolla, G.; White, A. J. P.; Williams, D. J.; Zanello, P. *Organometallics* **1997**, *16*, 2646−2650.
(37) Muller, T. J. J.; Lindner, H. J. *Chem. Ber.* **1996**, *129*, 607−613.
(38) Tykwinski, R. R.; Stang, P. J. *Organometallics* **1994**, *13*, 3203−3208.

Scheme 4

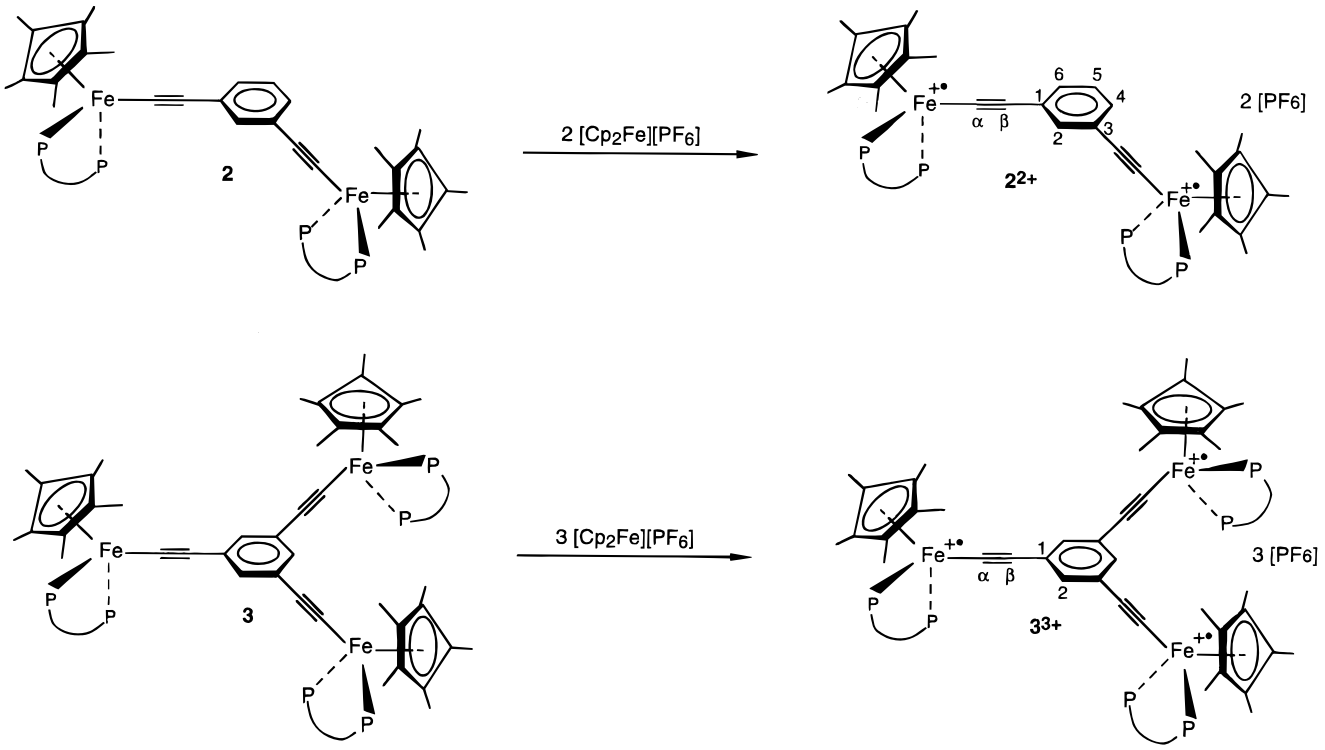

lecular distances. The intramolecular metal−metal interactions were experimentally characterized and compared with the results of DFT calculations. We now report (i) the synthesis of the bi- and trinuclear complexes $[\{Cp^*(dppe)Fe(C{\equiv}C-)\}_2(1,3\text{-}C_6H_4)][PF_6]_2$ ($\mathbf{2}^{2+}$) and $[\{Cp^*(dppe)Fe(C{\equiv}C-)\}_3(1,3,5\text{-}C_6H_4)][PF_6]_3$ ($\mathbf{3}^{3+}$), (ii) their optical properties together with comparisons with those of the related mononuclear complex $[Cp^*(dppe)Fe(C{\equiv}C-C_6H_5)][PF_6]$ ($\mathbf{1}^{+}$),[39] (iii) a paramagnetic ^1H NMR study showing that the molecule contains two equivalent iron centers that are magnetically different from the third one, (iv) a VT ^1H NMR study that is consistent with the interactions between the spin carriers mainly occurring through the bonds and suggesting that the zfs parameter *D* should be small, (v) ESR data that allowed the observation of the triplet and quartet states of these compounds, (vi) molar susceptibility measurements that show the ferromagnetic metal−metal exchange interaction, and (vii) the electronic structures of these open-shell derivatives obtained from density functional calculations.

Results and Discussion

1. Synthesis of the Iron(III) Bi- and Trinuclear Complexes $[\{Cp^*(dppe)Fe(C{\equiv}C-)\}_2(1,3\text{-}C_6H_4)][PF_6]_2$ ($\mathbf{2}^{2+}$) and $[\{Cp^*(dppe)Fe(C{\equiv}C-)\}_3(1,3,5\text{-}C_6H_3)][PF_6]$ ($\mathbf{3}^{3+}$). As previously reported, the neutral iron(II) complexes were obtained in one step by treatment of the iron chloro complex Cp*(dppe)FeCl (**5**) with 1 equiv of a precursor of the bridging ligands, namely, 1,3-bis(trimethylsilylethynyl)benzene or 1,3,5-tris(trimethylsilylethynyl)benzene. The reactions were carried out in a methanol/THF mixture (10:1) in the presence of KF and KPF_6, and the binuclear complex $\{Cp^*(dppe)Fe(C{\equiv}C-)\}_2(1,3\text{-}C_6H_4)$ (**2**) and its trinuclear analogue $\{Cp^*(dppe)Fe(C{\equiv}C-)\}_3(1,3,5\text{-}C_6H_3)$ (**3**) were obtained in 95 and 80% yields, respectively.[35] Due to low solubilities of the different organoiron compounds involved in the reactions, the oxidation of **2** and **3** must be carried out following the procedure carefully. The addition of 2 or 3 equiv of $[(C_5H_5)_2Fe][PF_6]$ to a CH_2Cl_2 suspension of $[\{Cp^*(dppe)Fe(C{\equiv}C-)\}_2(1,3\text{-}C_6H_4)]$ or $[\{Cp^*(dppe)Fe(C{\equiv}C-)\}_3(1,3,5\text{-}C_6H_3)]$, respectively, resulted in a rapid color change from orange to deep green, followed by a slower development of the final deep blue color (Scheme 4). After filtration of the solution to check that all the material was dissolved, the solvent was removed under vacuum. The solid was washed with diethyl ether to extract the ferrocene, and the measurement of the yield of the latter allowed a determination of the degree of completion of the reaction. Complexes $\mathbf{2}^{2+}$ and $\mathbf{3}^{3+}$ were isolated as thermally and air stable blue microcrystalline solids in 95 and 80% yields, respectively, after crystallization from CH_2Cl_2/pentane. The analytically pure salts $\mathbf{2}^{2+}$ and $\mathbf{3}^{3+}$, which showed the same cyclic voltammograms as the parent compounds **2** and **3** with two and three reversible waves, respectively,[35] were characterized by cyclic voltammetry, IR, UV−vis, ^1H NMR, Mössbauer, and ESR spectroscopies, and magnetochemistry.

Despite numerous efforts, it was not possible to grow single crystals of $\mathbf{3}^{3+}$. However, useful features on the trimetallic arrangement were drawn from the X-ray data obtained for the parent neutral complex **3**[35] since in the Cp*Fe(dppe) series it has been observed that the geometry of the iron(III) radical cation is not very different from that of their iron(II) homologues.[33,40] This

(39) Connelly, N. G.; Gamasa, M. P.; Gimeno, J.; Lapinte, C.; Lastra, E.; Maher, J. P.; Narvor, N. L.; Rieger, A. L.; Rieger, P. H. *J. Chem. Soc., Dalton Trans.* **1993**, 2575−2578.

(40) Roger, C.; Toupet, L.; Lapinte, C. *J. Chem. Soc., Chem. Commun.* **1988**, 713−715.

Scheme 5

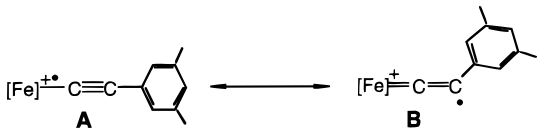

assumption is strongly supported by theoretical calculations (see section 9). As depicted in Figure 1, two iron centers of compound **3** (A and A′, Figure 1) have their Cp* ligands on one side of the molecule, whereas the Cp* ligand on the third iron atom (B) is located on the other side with an average distance between the iron(III) centers close to 10.4 Å. The three iron radicals make an almost isoceles triangle ABA′ in which the two edges AB and A′B are slightly longer than the third one AA′.

2. Infrared Spectroscopy. The IR spectra of the di- and trication complexes $\mathbf{2}^{2+}$ and $\mathbf{3}^{3+}$ in a CH_2Cl_2 solution display a single $\nu_{(C\equiv C)}$ stretching band similar to the mononuclear iron(III) complex [Cp*(dppe)Fe−C≡C−C_6H_5][PF_6] ($\mathbf{1}^+$, see Table 1).[39] Comparison of the IR data with those of the related neutral iron(II) species **2** and **3** shows that the one-electron oxidation of all the metal centers produces a decrease of the carbon−carbon triple-bond stretching of 27, 41, and 44 cm^{-1} for the mono-, bi-, and trinuclear complexes, respectively. The lower stretching frequencies observed in the oxidized compounds suggest a diminution of the bond order for the C≡C triple bond and, as a consequence, an increase of the bond order for the Fe−C bonds in agreement with the DFT calulations (vide infra). A weak contribution of an allenylidene-type resonance structure with a carbon-centered radical (form B in Scheme 5) to the bonding description of this family of iron(III) complexes is in agreement with the IR data and also confirmed by the calculations (vide infra), although form **A** is preponderant.

It is noteworthy that this effect increases with the number of organometallic building blocks connected to the arene ring, indicating that interactions between the metal centers occur through the organic spacer. It can also be noted that the diminution of the frequency of the $\nu_{(C\equiv C)}$ bond is not as large as that found for the binuclear derivative [{Fe(Cp*)(η^2-dppe)(C≡C−)}$_2$(1,4-C_6H_4)] ($\Delta\nu_{(C\equiv C)}$ = 69 cm^{-1})[32] for which the two organometallic building blocks are connected by the 1,4-diethynylbenzene spacer.

3. Optical Properties. The UV−vis spectra of the diamagnetic complexes **2** and **3** and their Fe(III) paramagnetic homologues $\mathbf{2}^{2+}$ and $\mathbf{3}^{3+}$ were recorded in CH_2Cl_2. The two neutral complexes showed two intense absorptions at λ (ϵ, M^{-1} cm^{-1}), 254 nm (28 000), and 349 nm (15 000) for the binuclear compound and at λ 283 nm (53 400) and 351 nm (35 000) for the trimetallic complex. The second absorption band tails in the visible for both compounds, but no maxima were detected in this region of the spectra. In contrast, the spectra of the deep blue radicals displayed two maxima in the visible range at 574 nm (4500), 662 nm (4500) and 573 nm (5500), 662 nm (5500) for $\mathbf{2}^{2+}$ and $\mathbf{3}^{3+}$, respectively. A single intense absorption band is also observed in the UV ($\mathbf{2}^{2+}$, 285 nm (57 700); $\mathbf{3}^{3+}$, 288 nm (55 700)). The electronic spectra of the reference compounds [Cp*(dppe)Fe−C≡C−C_6H_5)][PF_6]$_n$ (**1**, n = 0; $\mathbf{1}^+$ n = 1) were also investigated. Two absorptions were observed for the neutral iron(II) complex (λ (ϵ, M^{-1} cm^{-1}), 245 nm (34 300), and 348 nm (11 800), whereas the iron(III) derivative was characterized by four bands (241 nm (34 300), 267 nm (27 600), 575 nm (2200), and 663 nm (2900)). As usual for organometallic compounds, the absorptions in the range 240−280 nm are associated with $\pi-\pi^*$ transitions in the ligands. In the Fe(III) complexes $\mathbf{1}^+$, $\mathbf{2}^{2+}$, and $\mathbf{3}^{3+}$ the broad absorption bands observed at low energy (550−700 nm) may be attributed to ligand-to-metal charge transfer (LMCT) transitions from low-lying ligand-based molecular orbitals (MO) to the partially filled HOMOs, which are mainly metallic in character (see section 9).[41,42] It is noteworthy that these transitions occur at the same wavelengths in the three cases, indicating that the energy differences between the involved ligand-based and metal-based MOs are roughly the same in the three radicals.

Table 1. IR $\nu_{C\equiv C}$ Bond Stretching and Mössbauer Parameters for the Mono-, Bi-, and Trinuclear Fe(II) and Fe(III) Complexes

	IR (cm^{-1})		Mössbauer (mm s^{-1} vs Fe, 80 K)	
compd	Nujol	CH_2Cl_2	QS	IS
$\mathbf{1}^+$	2022		0.90	0.27
1	2049		2.00[a]	0.27[a]
$\mathbf{2}^{2+}$	2007	2006	0.89	0.28
2	2053	2049	2.00[a]	0.20[a]
$\mathbf{3}^{3+}$	2012	2010	0.88	0.25
3	2051	2050	1.99[a]	0.26[a]

[a] From ref 35.

4. Mössbauer Spectroscopy. Mössbauer spectroscopy is a very powerful tool for the determination of the oxidation state of iron in its complexes. The isomer shift and the quadrupole splitting (QS) are very sensitive to the spin and oxidation state of the iron centers.[43,44] The quadrupole splitting of ^{57}Fe Mössbauer spectra of crystallized samples of $\mathbf{2}^{2+}$ and $\mathbf{3}^{3+}$ recorded at zero field are characteristic of pure low-spin iron(III) complexes and compare well with those of the mononuclear species $\mathbf{1}^+$ (Table 1). As previously reported for other mononuclear iron(III) complexes in the half-sandwich Cp*(dppe)Fe series, the single quadrupole doublet is temperature-independent between 80 and 300 K and the parameters are well differentiated from those of the iron(II) complexes.[45] These spectra confirm that the isolated bi- and trication $\mathbf{2}^{2+}$ and $\mathbf{3}^{3+}$ are free of iron(II) impurities and establish the low-spin iron(III) character of the metal centers. Moreover, in the experimental uncertainty the QS values of the three iron(III) complexes $\mathbf{1}^+$, $\mathbf{2}^{2+}$, and $\mathbf{3}^{3+}$ are not sigificantly different, indicating that the metal environment is very similar for the three iron(III) complexes.

5. NMR Study of the Paramagnetic Complexes. The ^{1}H 300 MHz NMR spectra of the three complexes $\mathbf{1}^+$, $\mathbf{2}^{2+}$, and $\mathbf{3}^{3+}$ in CH_2Cl_2 solution were recorded at 20 °C. Complete assignment of the spectrum of $\mathbf{1}^+$ was

(41) Maestri, M.; Balzani, V.; Deuschel-Cornioley, C.; Von Zelewsky, A. *Adv. Photochem.* **1992**, *17*, 1.
(42) Schmid, B.; Garces, F. O.; Watts, R. J. *Inorg. Chem.* **1994**, *33*, 9−14.
(43) Greenwood, N. N. *Mössbauer Spectroscopy*; Chapman and Hall: London, 1971.
(44) Guillaume, V.; Thominot, P.; Coat, F.; Mari, A.; Lapinte, C. *J. Organomet. Chem.* **1998**, *565*, 75−80.
(45) Roger, C.; Hamon, P.; Toupet, L.; Rabaâ, H.; Saillard, J.-Y.; Hamon, J.-R.; Lapinte, C. *Organometallics* **1991**, *10*, 1045−1054.

Table 2. ^{1}H NMR of the Fe(III) Complexes 1^+, 2^{2+}, and 3^{3+}, 293 K, CD_2Cl_2

		CH_2		phenyl of the dppe ligand						
compd	Cp*	a	b	*o*	*m*	*p*	*o′*	*m′*	*p′*	central arene
1^+	−10.52	−2.84	1.79	6.75	6.19		3.60	7.87		7.03−7.56
2^{2+}	−10.90	−2.97	6.10	6.79	6.43		3.47	7.88		7.27−7.61
3^{3+}	−11.12	−3.05	2.34	6.88	6.09		3.38	7.81		7.28?
	−11.42	−2.88	2.51							

achieved by recording the spectra of different samples of the Fe(III) complex containing various molar ratios of the corresponding Fe(II) analogue. As previously observed for alkyl complexes on the same iron series,[45] a fast electron exchange occurs between these Fe(II) and Fe(III) species in the NMR time scale, and as a result, a single set of peaks was observed. A linear relationship between the observed chemical shifts and the molar ratio of the diamagnetic and paramagnetic compounds **1** and 1^+ was established. This correlation between the chemical shifts of these two species allowed the assignments given in Table 2. The binuclear complex 2^{2+} displayed a ^{1}H NMR spectrum very similar to that of 1^+, and assignment of the resonances was done by comparison of the spectra. In the upfield region, an intense and broad signal corresponding to the five methyl groups of the Cp* is observed below δ −10 ppm. Depending on their orientation toward the coupling unit or to the outside of the molecule, two different methylene and phenyl groups exist in the molecule. The two types of methylene protons are shifted upfield and downfield, and this effect is stronger for the binuclear compound 2^{2+}. In the downfield region, four signals are assigned to the *p′*, *o*-*m*, *p*, and *o′*-*m′* protons of the phenyl groups of dppe, and an unresolved multiplet corresponding to the ethynyl arene was also found. Note that the *o′* and *m′* protons are strongly downfield shifted in the paramagnetic complexes compared to the same resonances of their neutral diamagnetic parents. Moreover, selective irradiations at δ 3.5 and 6.9 ppm confirmed the assignments of the *p* and *p′* proton resonances of the phenyl group of the dppe.

The ^{1}H NMR spectrum of the trinuclear derivative 3^{3+} presents an interesting particularity. The peaks corresponding to the Cp* and methylene resonances are clearly split into two signals in 2:1 ratio (Table 2). The explanation for this observation can be found by examining the molecular structure of the corresponding neutral trinuclear complex **3** shown in Figure 1. Two of the Cp* groups are disposed on one face of the molecule, whereas the third one is positioned on the other side. Due to their steric bulk, the three organoiron groups cannot all be located on the same side of the molecule at the same time and their rotation should be concerted. As a consequence, the two faces of the molecule are magnetically nonequivalent. In the diamagnetic complex **3**, it was not possible to observe two sets of resonances in the ^{1}H spectrum, but two different resonances were found for the ^{31}P nuclei.[35] The range of the chemical shifts being much larger in the paramagnetic compounds, the Cp* and CH_2 resonances of both faces of the trication 3^{3+} are separated, but the arrangement of the organoiron groups is expected to be the same as that in the diamagnetic neutral complex.

6. Curie Law and Line Broadening. For paramagnetic compounds, the observed isotropic shift may

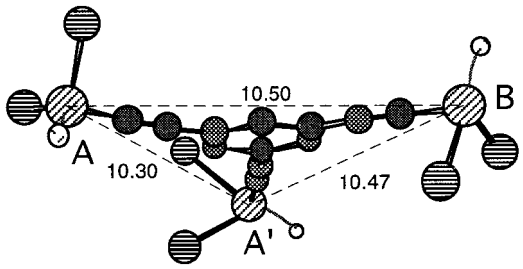

Figure 1. Molecular model of triradical 3^{3+} based on the structure of the trinuclear neutral homologue **3**.[35] For clarity, only the atoms bounded directly to the metal centers are shown. The Cp* groups are represented by their centroids, two of them being located below the plane ABA′ and the third one on the opposite side. The dashed lines indicate the iron−iron distances.

arise from contact and/or dipolar interaction (eq 1).[46]

$$\delta_{obs} = \delta_{iso} + \delta_{dia} = \delta_{contact} + \delta_{dipolar} + \delta_{dia} \qquad (1)$$

For simple mononuclear systems with one unpaired electron ($S = 1/2$) such as 1^+, both contact and dipolar terms are expected to have inverse temperature dependence.[47] However, for $S > 1/2$ compounds, the zero field splitting (zfs) can also lead to dipolar shift with a T^{-2} temperature dependence.[48] The presence of simultaneous contact and dipolar contributions to the observed isotropic shifts can be established by detection of curvature in a Curie plot.[49] The resolution of the ^{1}H NMR spectra of the iron(III) derivatives 2^{2+} and 3^{3+} rapidly decreases with the temperature, a large broadening of most of the resonances being observed and they overlay each other. As a result, only the protons of the Cp* and the downfield CH_2 signals are observable in the range 200−300 K. However, in the case of the trinuclear complex 3^{3+} the two nonequivalent Cp* resonances also overlay below 250 K, and for this reason, we only considered the most intense signal in the following. The observed isotropic shifts for these two resonances were plotted vs T^{-1} for both resonances of both iron(III) complexes (Figure 2). For the two compounds linear relationships were found which extrapolate through the origin within experimental error for the Cp* ligand, indicating that the Curie law is accurately obeyed. Consequently, the shifts of the protons of the Cp* should be essentially contact in origin and the zfs parameters, *D*, for 2^{2+} and 3^{3+} are expected to be small. Moreover, we note that relative shifts for the monomer, dimer, and trimer are quite similar in this series, and consequently, the mode of spin-delocalization is probably the same for the three complexes.[50] The behavior of the methylene protons that are separed from the metal centers by three σ bonds is different. Although the isotropic shifts vary linearly with inverse temperature, the extrapolated intercepts are nonzero.

(46) Bertini, I.; Luchinat, C. *NMR of Paramagnetic Molecules in Biological Systems*; The Benjamin/Cummings Publishing Co., Inc.: Menlo Park, CA, 1986.

(47) Basu, P.; Shokhirev, N. V.; Enemark, J. H.; Walker, F. A. *J. Am. Chem. Soc.* **1995**, *117*, 9042−9055.

(48) Wicholas, M.; Mustacich, R.; Jayne, D. *J. Am. Chem. Soc.* **1972**, *94*, 4518−4522.

(49) La Mar, G. N.; Eaton, G. R.; Holm, R. H.; Walker, F. A. *J. Am. Chem. Soc.* **1973**, *95*, 63−75.

(50) It was previously concluded that the dipolar contribution to the isotropic shifts in iron(III) alkyl complexes was small.[45]

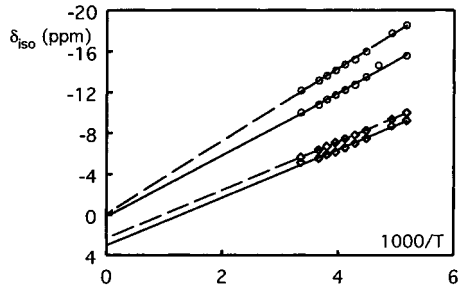

Figure 2. Plot of the temperature dependence of the isotropic shifts of the Cp* ligand (circles) and the upfield methylene protons of the dppe (squares) for $\mathbf{2}^{2+}$ (dashed line) and $\mathbf{3}^{3+}$ (solid line). The curves were obtained from a linear fit of the experimental data (circles).

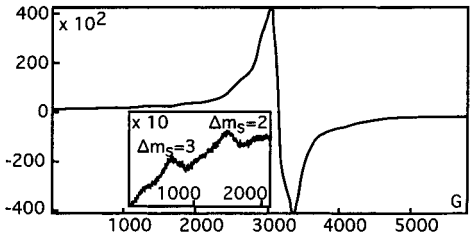

Figure 3. ESR spectrum of $\mathbf{3}^{3+}$ in rigid glass (CH_2Cl_2/$C_2H_4Cl_2$, 1:1) at 77 K.

This suggests a dipolar contribution to the shift of these protons. The dipolar shift depends on the orientation of the ligands with respect to the magnetic axis of the molecule,[47] and one can see from Table 2 that the chemical shifts of the methylene proton in *endo* or *exo* positions are quite different.

7. ESR Measurements. The low-temperature ESR spectrum of the iron(III) alkynyl complex $\mathbf{1}^{+}$ shows three well-separated features corresponding to the three components of the *g*-tensor.[39] In contrast, and as usual for a biradical, $\mathbf{2}^{2+}$ displayed an unresolved broad signal with $\Delta H_{pp} = 550$ G at $g = 2.10$ in a rigid glass (77 K, $CH_2Cl_2/C_2H_4Cl_2$, 1:1). The broadening of the signals is a consequence of the presence of several unpaired electrons in the same molecule, which greatly shortens the relaxation time. Moreover, a $\Delta m_s = 2$ transition characteristic of a triplet state is observed at $g = 4.55$. The ESR spectrum of the tris(iron) radical $\mathbf{3}^{3+}$ also exhibits an unresolved and broad signal with $\Delta H_{pp} = 330$ G at $g = 2.13$ (77 K, $CH_2Cl_2/C_2H_4Cl_2$, 1:1). In addition, two weak signals ($g = 4.46$ and 7.97) due to $\Delta m_s = 2$ and 3 transitions, respectively, are also observed (Figure 3). The spectrum recorded at 4 K under the same conditions shows slightly narrower line width and a weak variation of the *g* value ($\Delta H_{pp} = 170$ G, $g = 2.14$). In the range 90−160 K, the plot of intensity vs T^{-1} deviates upward from a linear relationship, suggesting a quartet ground state (Figure 4).

8. Magnetic Susceptibility Measurements. Magnetic measurements were carried out from 2 to 300 K. As the temperature increased, the effective moment μ_{eff} of the bis(iron) radical $\mathbf{2}^{2+}$ gradually increases from 1.93 μ_B at 2 K, reached a maximum of 2.36 μ_B at 24 K, and slowly decreased to 2.28 at 300 K, as shown in Figure 5. This complex variation of μ_{eff} with the temperature should be the consequence of competitive intra- and intermolecular exchange interactions. For a biradical with two $S = 1/2$ centers, the singlet−triplet separation

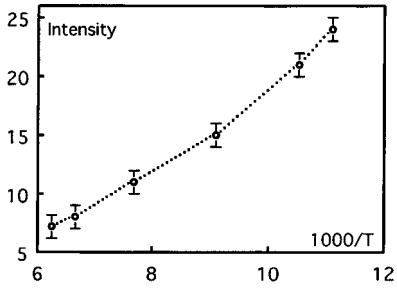

Figure 4. Plot of the $\Delta m_s = 2$ signal intensity (arbitrary unit) vs inverse temperature for $\mathbf{3}^{3+}$.

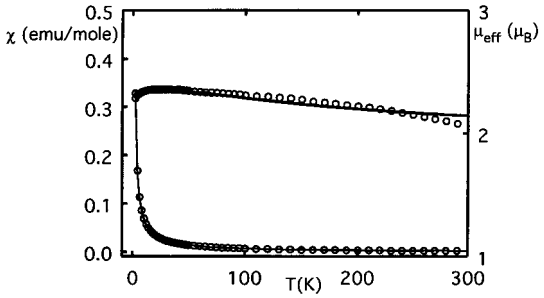

Figure 5. Temperature dependence of the molar magnetic susceptibility (χ) and the effective magnetic moment (μ_{eff}) for $\mathbf{2}^{2+}$. Solid lines are the theoretical curves calculated with eq 2 for $J/k = 94.0 \pm 0.1$ K and $\theta = -0.12 \pm 0.05$ K.

is given by the Bleaney−Bowers expression where $2J$ is the singlet−triplet energy gap (eq 2).[18,51]

$$\chi = \frac{2N\bar{g}^2\mu_B^2}{k(T-\theta)}\frac{1}{3+\exp(-2J/kT)} \qquad (2)$$

The experimental data were fitted with eq 2, and one set of parameters was obtained for assuming $g = 2.10$, $J/k = 94.0 \pm 0.1$ K, $\theta = -0.12 \pm 0.05$ K. The theoretical curve is shown by the solid line in Figure 5. As is very often the case, the negative θ value indicates that the interaction between molecules is weakly antiferromagnetic.[24] According to the positive *J* value, the complex $\mathbf{2}^{2+}$ has a triplet ground state, and the singlet−triplet energy gap $\Delta E_{TS} = 2J = 130.6 \pm 0.2$ cm^{-1}. Among the numerous examples of ferromagnetic coupling between organic biradicals connected with a *m*-phenylene spacer, significantly stronger couplings have been reported. However, in terms of strength of spin coupling in diradicals, an S−T splitting as large as 130 cm^{-1} is a quite surprising value with respect to the Fe···Fe separation, which is up to 10 Å. To our knowledge, the ferromagnetic coupling observed for $\mathbf{2}^{2+}$ is among the highest values reported for nanoscopic molecular devices.[26,52] Moreover, this result indicates that the high-spin topology rules[21] apply to charged organometallic polyradicals.

The temperature dependence of the magnetic susceptibility of the tris(iron) radical $\mathbf{3}^{3+}$ is shown in Figure 6. As the temperature increases, the effective moment increases from 2.92 μ_B at 2 K to a maximum of 3.03 μ_B at 20 K and then decreases to reach 2.33 μ_B at 300 K. The decrease of μ_{eff} above 20 K should be due to the thermal population of the excited doublet states from

(51) Bleaney, B.; Bowers, K. *Proc. R. Soc. London* **1952**, *A214*, 451.
(52) Rajca, A. *Chem. Rev.* **1994**, *94*, 871−893.

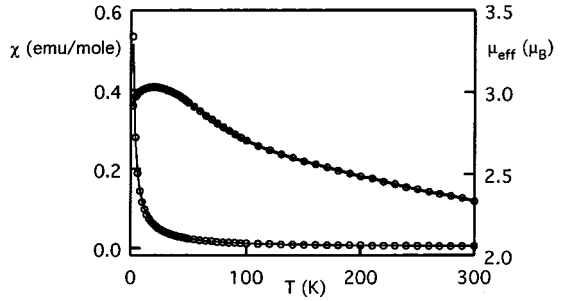

Figure 6. Temperature dependence of the molar magnetic susceptibility (χ) and the effective magnetic moment (μ_{eff}) for $\mathbf{3}^{3+}$. Solid lines are the theoretical curves calculated with eq 4 for $J/k = 13.7 \pm 0.1$ K, $\alpha = 0.48 \pm 0.02$, and $\theta = -0.46 \pm 0.05$ K.

the quartet ground state. The magnetic interactions in an isosceles triangular three-spin model are described by the following Heisenberg Hamiltonian (eq 3).[24,26]

$$H = -2J(S_{A1}S_B + S_BS_{A2} + \alpha S_{A1}S_{A2}) \quad (3)$$

The resulting states are two doublets ($S = 1/2$) and one quartet ($S = 3/2$), and the experimental molar magnetic susceptibility for this system can be expressed by eq 4. In these expressions $\alpha = J/J'$ (see Scheme 2). As previously established, the Hamiltonian described by eq 3 has the eigenvalues given in eq 5.[19]

$$\chi = \frac{N\bar{g}^2\mu_B{}^2}{4k(T-\theta)} \frac{1 + \exp(2(\alpha-1)J/kT) + 10\exp((1+2\alpha)J/kT)}{1 + \exp(2(\alpha-1)J/kT) + 2\exp((1+2\alpha)J/kT)} \quad (4)$$

$$E_{D2}(S = 1/2) = J(2 - \alpha/2)$$

$$E_{D1}(S = 1/2) = J(3\alpha/2)$$

$$E_Q(S = 3/2) = -J(1 + \alpha/2) \quad (5)$$

The magnetic susceptibility data of $\mathbf{3}^{3+}$ at 2−300 K were fitted to eq 4 by treating J, θ, and α as adjustable parameters. The g value was assumed to be equal to that obtained by ESR, i.e., $g = 2.13$. The calculated magnetic susceptibility shown by the solid line in Figure 6 was obtained for $J/k = 13.7 \pm 0.1$ K, $\alpha = 0.48 \pm 0.02$, $\theta = -0.46 \pm 0.05$ K. Since J is positive, the ground state consists of a quartet ground state ($S = 3/2$) and the two excited doublet states that lie above it by 18.7 $\pm$ 0.5 and 28.8 $\pm$ 0.5 cm^{-1}. This energy difference is significantly smaller than the ΔE_{TS} value found for $\mathbf{2}^{2+}$. Triradicals are relatively rare compared to diradicals. However, the ΔE_{QD} differences have been determined for few triradicals with a triangular topology. The magnetic couplings are either ferro-[9,19] or antiferromagnetic,[24] the strength of the coupling being generally stronger than in $\mathbf{3}^{3+}$, but weaker than in the corresponding diradicals.[26,52] In most of these triradicals, the distances between the spin carriers are much shorter than in our compound. Note also that once again the intermolecular interaction is antiferromagnetic.[1,19]

9. Theoretical Calculations. Density functional molecular-orbital calculations were carried out on the title compounds in order to further the understanding of their physical properties (see the Experimental Section for computational details). The model compounds [{Fe(Cp)$(PH_3)_2$(C≡C−)}$_2$(1,3-C_6H_4)] (**2-H**) and [{Fe(Cp)-$(PH_3)_2$(C≡C−)}$_3$(1,3,5-C_6H_3)] (**3-H**) were used to reduce computational effort.[35] For comparison, calculations were also performed on the models [{Fe(Cp)$(PH_3)_2$(C≡C−)}$_2$(1,4-C_6H_4)] (**4-H**) and [Fe(Cp)$(PH_3)_2$(C≡C−C_6H_5)] (**1-H**). Unless specified, partial optimization was made under the C_{2v}, C_{3v}, C_{2v}, and C_s symmetry constraint for the models **2-H**, **3-H**, **4-H**, and **1-H**, respectively. The results on the neutral molecules have been published previously.[35] For the sake of this discussion they are briefly recalled in Table 3 along with the results obtained for the cationic $(\mathbf{1\text{-}H})^+$, $(\mathbf{2\text{-}H})^{2+}$, $(\mathbf{3\text{-}H})^{3+}$, and $(\mathbf{4\text{-}H})^{2+}$ species. Spin-unrestricted calculations were carried out on the high- and low-spin (HS and LS) cationic models when the spin-up electrons outnumber the spin-down electrons. Spin-restricted calculations were carried out otherwise.

Table 3. Optimized Bond Distances (Å) and Bonding Energies (eV) for Neutral and Cationic Models 1-H, 2-H, 3-H, and 4-H

model	Fe−C(α)	C(α)−C(β)	C(β)−C(1)	C(1)−C(2)	BE[a]
1-H	1.901	1.239	1.434	1.402	−182.069
$(\mathbf{1\text{-}H})^+$	1.847	1.251	1.414	1.402	−176.051
2-H	1.879	1.235	1.423	1.405	−289.714
$(\mathbf{2\text{-}H})^{2+}$ (LS)[b]	1.842	1.250	1.414	1.408	−276.265
$(\mathbf{2\text{-}H})^{2+}$ (HS)[c]	1.842	1.247	1.415	1.407	−276.609
3-H	1.893	1.238	1.430	1.409	−397.264
$(\mathbf{3\text{-}H})^{3+}$ (LS)	1.856	1.248	1.417	1.411	−374.959
$(\mathbf{3\text{-}H})^{3+}$ (HS)	1.861	1.244	1.426	1.406	−375.364
4-H	1.882	1.236	1.423	1.405	−289.728
$(\mathbf{4\text{-}H})^{2+}$ (LS)	1.812	1.257	1.382	1.434 1.366[d]	−277.063
$(\mathbf{4\text{-}H})^{2+}$ (HS)	1.856	1.246	1.414	1.418 1.383[d]	−276.808

[a] Bonding energy (see ref 61). [b] Low-spin state. [c] High-spin state. [d] C(2)−C(3).

Regardless of the high- or low-spin configurations, the calculated geometries of the oxidized $(\mathbf{2\text{-}H})^{2+}$ and $(\mathbf{3\text{-}H})^{3+}$ species are not significantly different from those of the neutral (**2-H**) and (**3-H**) parents. The largest change occurs for the Fe−C(α) separations, which slightly shorten by ca. 0.03 Å upon the removal of electrons. The C−C bond distances are hardly affected (see Table 3). In particular, the C(α)−C(β) bonds lengthen by less than 0.01 Å. There are no significant differences between the bond lengths optimized for HS and LS configurations. These distances are comparable to those computed for the neutral and cationic compounds **1-H** and $(\mathbf{1\text{-}H})^+$.

Similarly, bond lengths computed for **4-H** and HS $(\mathbf{4\text{-}H})^{2+}$ do not differ significantly and are comparable to those obtained for **2-H** and $(\mathbf{2\text{-}H})^{2+}$ (see Table 3). Interestingly enough, a larger change is observed for the LS $(\mathbf{4\text{-}H})^{2+}$ model with respect to **4-H**. The Fe−C(α) and C(α)−C(β) distances shorten and lengthen by 0.07 and 0.02 Å, respectively. The C(β)−C(1) is shorter by 0.04 Å and the C(1)−C(2) bond length increases by 0.03 Å, whereas the C(2)−C(3) bond length of the arene ring decreases by 0.04 Å. This indicates that the quinone resonance structure is quite important in the bonding description of LS $(\mathbf{4\text{-}H})^{2+}$. In contrast, the HS $(\mathbf{4\text{-}H})^{2+}$ model is better described with the phenylene form. The change for the C(α)−C(β) distance in LS $(\mathbf{4\text{-}H})^{2+}$ is larger than the corresponding one in $(\mathbf{2\text{-}H})^{2+}$ and $(\mathbf{3\text{-}H})^{3+}$ and is in agreement with the $\nu_{(C\equiv C)}$ stretching frequencies

measured in complexes $\mathbf{2}^{2+}$, $\mathbf{3}^{3+}$, and $\mathbf{4}^{2+}$. In the latter compound, a larger decrease of the $\nu_{(C\equiv C)}$ is observed between the neutral and dication species (see section 2).

These $\nu_{(C\equiv C)}$ stretching frequencies must be sensitive to the nature of electronic interactions with the metallic fragments. Previous calculations of the Fenske−Hall type supported by photoelectron spectroscopy measurements performed on $Fe(Cp)(CO)_2(C\equiv C-R)$ indicate that the predominant Fe−C π-type interactions are filled/filled interactions between occupied acetylide and metal π-orbitals and that the metal-to-acetylide-π^* back-bonding is extremely small.[53,54] An extended Hückel (EH) fragment analysis carried out on the different models that we studied also shows that the main metal−carbon π interactions are filled/filled interactions. Nevertheless, the replacement of CO ligands by phosphine ligands raises somewhat the energy of the metal dπ orbitals away from the occupied π-orbitals and closer to the vacant π^* orbitals of the ethynylbenzene ligand. Consequently, weaker filled/filled interactions and stronger filled/vacant interactions must occur, enhancing π^* back-donation. This is reflected in the Fe−C and C≡C bond lengths which are slightly shorter and longer, respectively, in our neutral molecules than in the $Fe(Cp)(CO)_2(C\equiv C-R)$ species.[54] The Fe−C and C−C bond lengths computed for the oxidized species thus depend on two effects which lead to some Fe−C shortening and C−C lengthening: the depopulation of Fe−C π-antibonding orbitals and the magnitude of π^* back-donation. These two effects are not easily separated. Nevertheless, an EH fragment analysis performed on the DFT-optimized cationic structures indicates that the electron back-donation per metal fragment is larger in the $(\mathbf{4\text{-}H})^{2+}$ species (0.30 electron) than in the $(\mathbf{2\text{-}H})^{2+}$, $(\mathbf{3\text{-}H})^{3+}$, and $(\mathbf{1\text{-}H})^{+}$ species (0.24, 0.23, and 0.25 electron, respectively). This weak but significantly larger π^* back-donation from the metal fragment toward the ethynylbenzene ligand in $(\mathbf{4\text{-}H})^{2+}$ with respect to that computed in $(\mathbf{2\text{-}H})^{2+}$, $(\mathbf{3\text{-}H})^{3+}$, and $(\mathbf{1\text{-}H})^{+}$ adds further support that the vinylidene resonance form contributes more in the bonding description of the former than in that of the latter models.

In accord with the ferromagnetic behavior observed for compounds $\mathbf{2}^{2+}$ and $\mathbf{3}^{3+}$, the lowest energies are achieved in the high-spin configurations for $(\mathbf{2\text{-}H})^{2+}$ and $(\mathbf{3\text{-}H})^{3+}$. For $(\mathbf{2\text{-}H})^{2+}$, the triplet state associated with the $(b_1)^1(a_2)^1$ electronic configuration is preferred by 0.344 eV (33 kJ/mol) over the singlet state, which is associated with the electronic $(b_1)^2(a_2)^0$ configuration. In the case of $(\mathbf{3\text{-}H})^{3+}$, the doublet state ($(a_2)^1(e)^2$ electronic configuration) is 0.405 eV (39 kJ/mol) higher in energy than the quartet state ($(a_2)^1(e)^2$ electronic configuration). In contrast, the lowest energy state is the singlet state ($(a_1)^2(a_2)^0$ electronic configuration) for $(\mathbf{4\text{-}H})^{2+}$. The high-spin state ($(b_1)^1(a_2)^1$ electronic configuration) is 0.255 eV (25 kJ/mol) higher in energy.

The energies of the frontier molecular orbitals of the LS and HS $(\mathbf{2\text{-}H})^{2+}$ and $(\mathbf{3\text{-}H})^{3+}$ models are shown in Figures 7 and 8, respectively. The orbitals are labeled according to the C_{2v} and C_{3v} irreducible representations

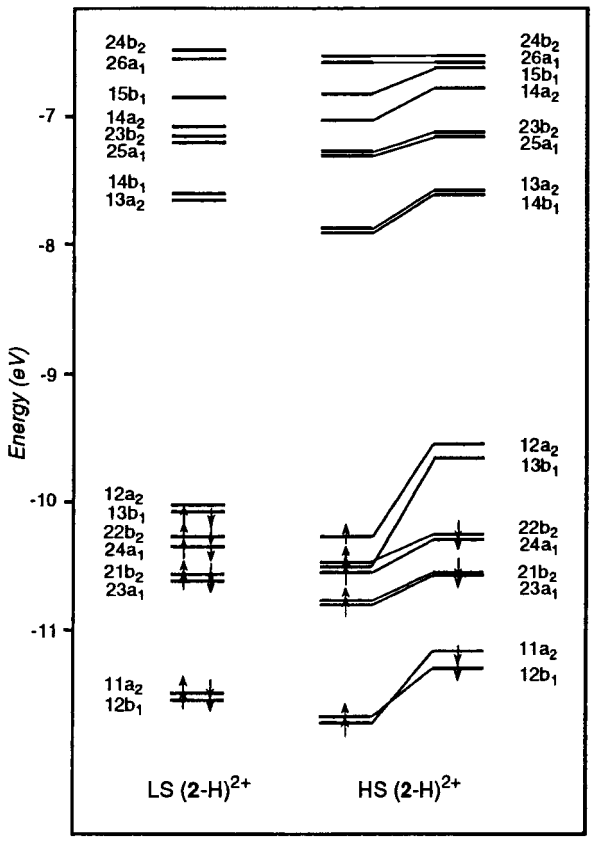

Figure 7. Spin-restricted orbital diagram for LS $(\mathbf{2\text{-}H})^{2+}$ (left-hand side) and spin-unrestricted orbital diagram for HS $(\mathbf{2\text{-}H})^{2+}$ (right-hand side) (only orbitals in the HOMO−LUMO region are shown).

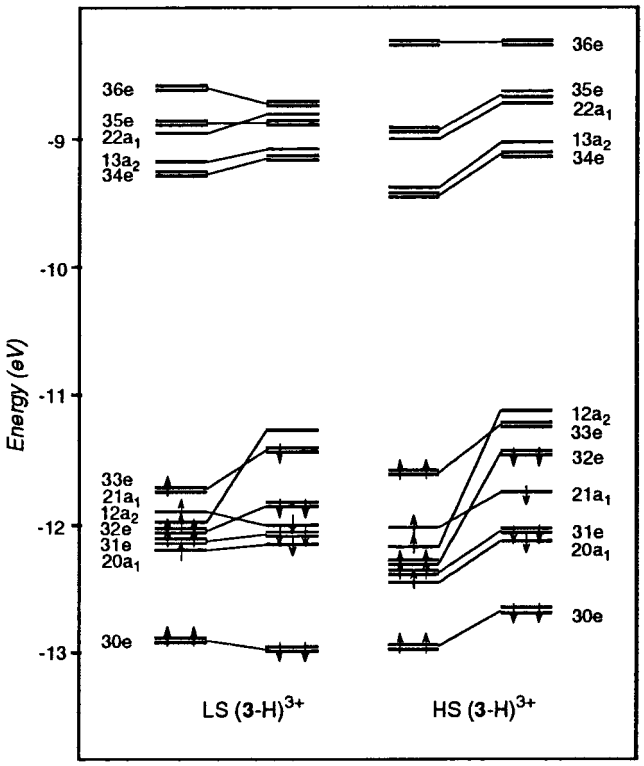

Figure 8. Spin-unrestricted orbital diagram for LS (a) and HS (b) $(\mathbf{3\text{-}H})^{3+}$ models (only orbitals in the HOMO−LUMO region are shown).

that they span for $(\mathbf{2\text{-}H})^{2+}$ and $(\mathbf{3\text{-}H})^{3+}$, respectively. The use of the spin-unrestricted approach doubles the

(53) Kostic, N. M.; Fenske, R. F. *Organometallics* **1982**, *1*, 974−982.
(54) Lichtenberger, D. L.; Renshaw, S. K.; Bullock, R. M. *J. Am. Chem. Soc.* **1993**, *115*, 3276−3285.

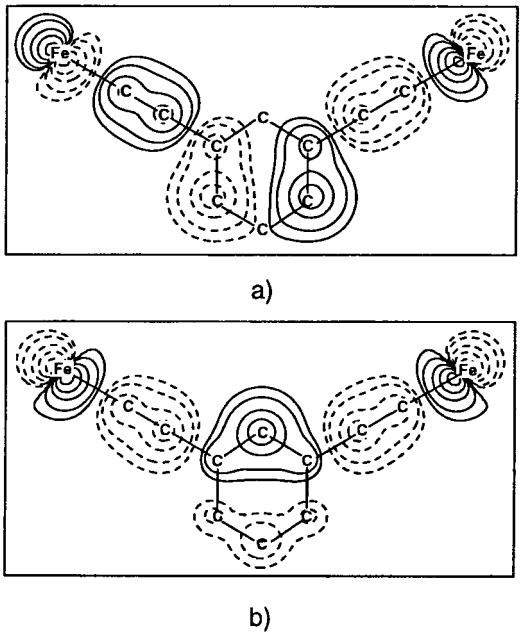

Figure 9. Contour plots (top view) 0.25 Å above the molecular plane of the highest occupied spin-up orbitals $12a_2$ (a) and $13b_1$ (b) of HS $(\mathbf{2\text{-}H})^{2+}$. Contour values are ±0.01, ±0.02, ±0.05, ±0.1, ±0.2, and ±0.5 [e/bohr^3]$^{1/2}$.

number of levels since spin-up and spin-down electrons occupying a molecular orbital are not constrained to have the same spatial wave function. Starting from the neutral species, electrons have been removed from the HOMOs $12a_2$ and $13b_1$ in $(\mathbf{2\text{-}H})^{2+}$ and from the HOMOs $12a_2$ and 33e in $(\mathbf{3\text{-}H})^{3+}$ upon oxidation.

The highest occupied spin-up orbitals are sketched in Figures 9 and 10 for the HS $(\mathbf{2\text{-}H})^{2+}$ and $(\mathbf{3\text{-}H})^{3+}$ species, respectively (the corresponding spin-down orbitals are vacant). Their spatial distribution mainly resembles that of the HOMOs computed for the neutral complexes.[35] As said earlier, a fragment analysis reveals that in $(\mathbf{2\text{-}H})^{2+}$ these orbitals result from antibonding interactions between dπ orbitals of the $Fe(Cp)(PH_3)_2$ fragments and out-of-plane π orbitals of the bis(ethynyl)-benzene ligand. The spin-up orbital $12a_2$ is rather delocalized over the whole molecule with a distribution of 44% Fe, 7% C(α), 17% C(β), and 20% C(4) (see Scheme 4 for the labels). The distribution is computed to be 52% Fe, 19% C(β), and 10% C(2) in character for the spin-up orbital $13b_1$. In the triradical $(\mathbf{3\text{-}H})^{3+}$ model, the three spin-up orbitals $12a_2$ and 33e spread out in the plane of the tris(ethynyl)benzene ligand. They mainly result from the antibonding interaction between metal dπ orbitals of the $Fe(Cp)(PH_3)_2$ fragments and in-plane π/σ orbitals of the tris(ethynyl)benzene ligand. These MOs contain several nodes and overall are strongly localized on the Fe centers (ca. 60%) and to a lesser extent on the ethynyl groups (ca. 5% on C(α) and 20% on C(β)), but rather poorly localized on the phenyl ring (less than 2%).

The spin density in HS $(\mathbf{2\text{-}H})^{2+}$ and $(\mathbf{3\text{-}H})^{3+}$ plotted in Figure 11 comes mainly from these occupied spin-up orbitals. In the case of HS $(\mathbf{2\text{-}H})^{2+}$, the spin density is spread out mainly in space perpendicular to the plane of the bis(ethynyl)benzene ligand. Important spin density is observed on the iron atoms and to a lesser extent on the C(β) carbon atoms and three carbon atoms

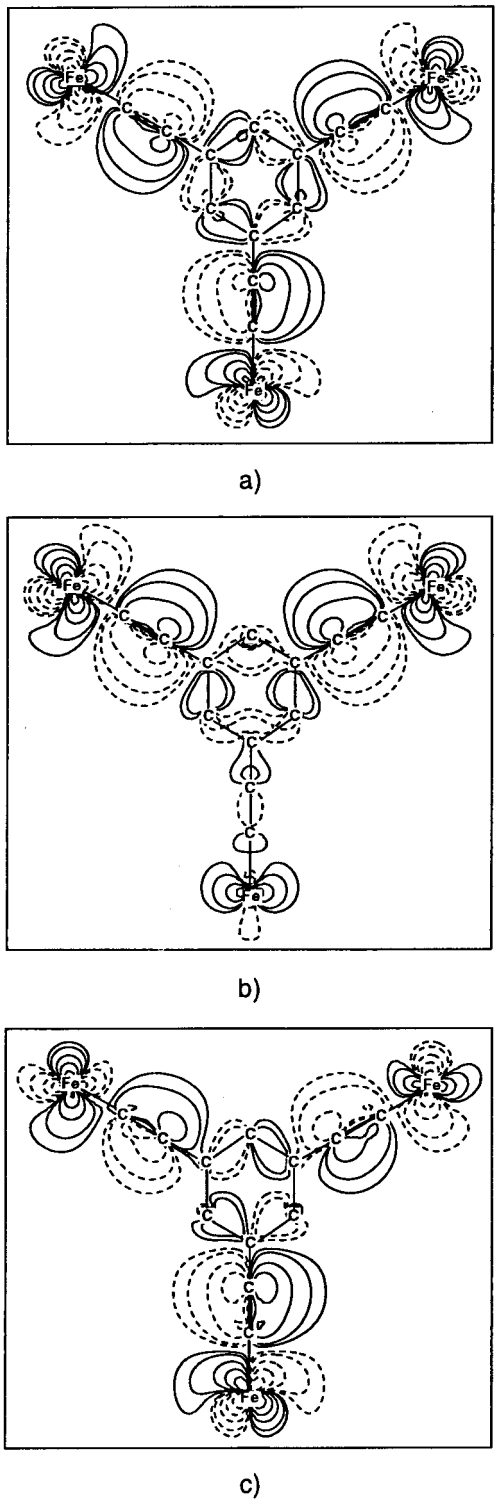

Figure 10. Contour plots (top view) in the molecular plane of the highest occupied spin-up orbitals $12a_2$ (a) and 33e (b and c) of HS $(\mathbf{3\text{-}H})^{3+}$. See caption to Figure 9 for contour values.

of the phenyl ring. A Mulliken spin population analysis indicates a population of 0.65, 0.25, and 0.16, respectively. In contrast, the spin density is somewhat less delocalized and distributed in the plane of the tris-(ethynyl)benzene ligand with a large amount spread over the iron centers, and to a lesser extent over the C(β) carbon atoms in HS $(\mathbf{3\text{-}H})^{3+}$. The spin population on each Fe and C(β) center is 0.80 and 0.29 electron, respectively. A few percent of positive spin density is

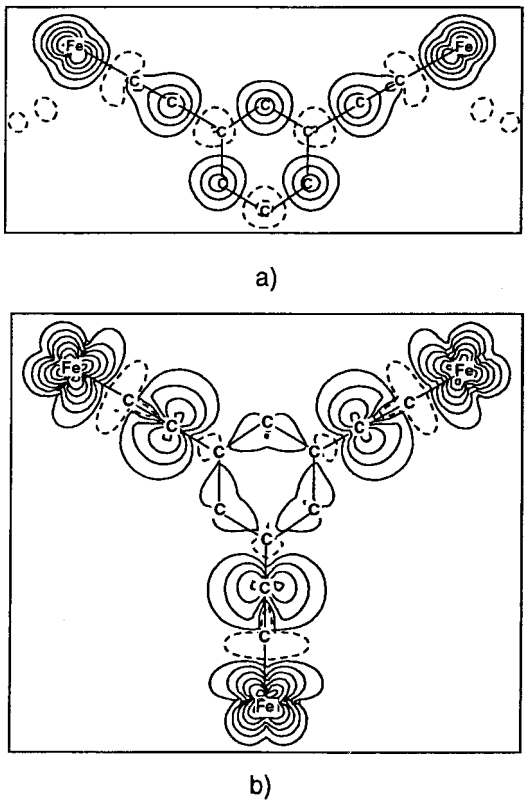

Figure 11. Plot of the positive (solid line) and negative (dashed line) spin density for (a) HS (**2-H**)$^{2+}$ (0.25 Å above the molecular plane) and HS (**3-H**)$^{3+}$ (in the molecular plane). Contour values are ±0.001, ±0.005, ±0.015, ±0.040, ±0.1, and ±0.25 [e/bohr^3].

also observed around three carbon atoms (one over two) of the phenyl ring. Weak negative spin density is localized on the other carbon atoms of the molecular core in (**2-H**)$^{2+}$ and (**3-H**)$^{3+}$ (see Figure 11). For comparison, the spin populations computed for (**1-H**)$^{+}$ are 0.59 and 0.19 on Fe and C(β), respectively. Some spin density is also distributed on C(α) (0.08) and the carbon atoms of the phenyl ring, particularly that in the *para* position to the ethynyl-iron group (0.12). This result indicates that the spin density is more delocalized in the monomeric species (**1-H**)$^{+}$ than in the dimeric and trimeric species (**2-H**)$^{2+}$ and (**3-H**)$^{3+}$. For all magnetic compounds, a very weak amount of spin density (less than 1%) is computed for the Cp rings tethered to the iron centers.

It seems that with such a spin distribution, Ovchinnikov's rule previously established for ferromagnetic organic spin carriers can be applied to the cationic organometallic compounds (**2-H**)$^{2+}$ and (**3-H**)$^{3+}$. Indeed, the metal−carbon backbone of the biradical (**2-H**)$^{2+}$ and triradical (**3-H**)$^{3+}$ species can be considered as alternant π-systems which can be divided in sets of starred and nonstarred atoms.[20−22] With the iron centers being starred, the number of starred atoms outnumbers the number of nonstarred atoms by 2 and 3 in (**2-H**)$^{2+}$ and (**3-H**)$^{3+}$, respectively. As expected from Ovchinnikov's topological rule, the triplet and quartet ground states are observed for (**2-H**)$^{2+}$ and (**3-H**)$^{3+}$, respectively, and the spin density resides mainly on the starred atoms (see above). In contrast, the two iron centers cannot both be starred in complex (**4-H**)$^{2+}$, and no ferromagnetism is observed.

In summary, optimized bond lengths and spin density localization computed for the cationic models (**2-H**)$^{2+}$ and (**3-H**)$^{3+}$ brings additional supporting evidence that the radical resonance structure **A** shown in Scheme 5 can be used to describe the bonding in the title compounds. The theoretical results also support the fact that oxidation of the neutral species **2** and **3** involves primarily removal of metal-based electrons, leading formally to 17-electron radical iron centers, as suggested by the experimental data.

Finally, the robust organometallic bi- and triradical **2**$^{2+}$ and **3**$^{3+}$ both have a ferromagnetic coupling with a magnetic interaction of significant strength at nanoscale distances. Clearly, we have shown that connection of 17-electron [Cp*(dppe)Fe(C≡C)−]$^{\bullet+}$ units through a phenyl ethynyl bridge allows nanosized magnetic interactions. Further development of the synthetic chemistry allowing introduction of these organoiron units into various organic environments of increased size will be the subject of future reports from our group.

Experimental Section

General Data. Reagent grade tetrahydrofuran (THF), diethyl ether, and pentane were dried and distilled from sodium benzophenone ketyl prior to use. Pentamethylcyclopentadiene was prepare according to the published procedure,[55] and other chemicals were used as received. All the manipulations were carried out under an argon atmosphere using Schlenk techniques or in a Jacomex 532 drybox filled with nitrogen. Routine NMR spectra were recorded using a Bruker AW 80 spectrometer. High-field NMR spectra experiments were performed on a multinuclear Bruker WB 300 instrument. Chemical shifts are given in parts per million relative to tetramethylsilane (TMS) for ^{1}H and ^{13}C NMR spectra and H_3PO_4 for ^{31}P NMR spectra. Cyclic voltammograms were recorded with a PAR 263 instrument. Mössbauer spectra were recorded with a 2.5×10^{-2} C (9.25×10^8 Bq) ^{57}Co source using a symmetric triangular sweep mode. X-band ESR spectra were recorded on a Bruker ESP-300E spectrometer at 77 K in liquid nitrogen. An Air Products LTD-3-110 liquid helium transfer system was attached for the low-temperature measurements. Magnetic susceptibility measurements were performed with a SQUID (Susceptometer Quantum Interface Device) instrument. Data were corrected for magnetization of the sample holder and capsule used, and diamagnetic contributions were estimated from Pascal's constants. The interatomic distances have been measured with the molecular modeling system Chem3D from Cambridge Scientific Computing. Elemental analyses were performed at the Center for Microanalyses of the CNRS at Lyon-Solaise, France.

[{Cp*(dppe)Fe(C≡C)}$_2$(1,3-C$_6$H$_4$)][PF$_6$]$_2$ (2^{2+}). To 0.190 g of [{Cp*(dppe)Fe(C≡C)}$_2$(1,3-C$_6$H$_4$)] in 20 mL of CH_2Cl_2 was added 0.075 g (1.95 equiv) of ferricinium salt. The mixture was stirred for 5 h at room temperature. The initially orange solution turned rapidly to blue. The solution was filtered and the solvent removed under vacuum. The blue solid was washed with cold pentane (2 × 10 mL) and dried. Recrystallization at low temperature (−70 °C) from CH_2Cl_2/pentane gave 0.225 g (1.4×10^{-4} mol) of blue crystals of the bicationic complex [{Cp*(dppe)Fe(C≡C)}$_2$(1,3-C$_6$H$_4$)][PF$_6$]$_2$ (95% yield). Anal. Calcd for $C_{82}H_{82}F_{12}Fe_2P_6$: C, 61.8; H, 5.19. Found: C, 61.7; H, 5.29. FT-IR (Nujol, cm^{-1}): 2007 (νC≡C). ^{1}H NMR (300 MHz, CD_2Cl_2) δ_H 7.88 (s, 4H, *p*-Ph), 7.61−7.27 (m, 4H,

(55) Kohl, F. X.; Jutzi, P. *J. Organomet. Chem.* **1983**, *243*, 119−125.

(56) For an introduction to density functional theory, see for example refs 57−60.

1,3-C_6H_4), 6.79 (s, 16 H, *o′,m′*-Ph), 6.43 (s, 4H, CH_2), 6.10 (s, 4H, *p′*-Ph), 3.47 (s, 16 H, *o,m*-Ph); −2.97 (s, 4H, CH'_2), −10.90 (s, 30H, C_5Me_5). Mossbaüer (mm/s vs Fe, 77 K): IS 0.28, QS 0.89. UV (CH_2Cl_2): λ_{max} (ϵ/10^3 dm^3 mol^{-1} cm^{-1}) = 285(57.7), 574(4.5), 662(4.5).

[{Cp*(dppe)Fe(C≡C)}$_3$(1,3,5-C_6H_3)][PF_6]$_3$ (3^{3+}). To 0.225 g of [{Cp*(dppe)Fe(C≡C)}$_3$(1,3,5-C_6H_3)] in 20 mL of CH_2Cl_2 was added 0.113 g (2.95 equiv) ferricinium salt. The mixture was stirred during 6 h at room temperature. The initially orange solution turned rapidly to blue. The solution was filtered and the solvent removed under vacuum. The blue solid was washed with cold pentane (2 × 10 mL) and dried. Recrystallization at −70 °C from CH_2Cl_2/pentane gave 0.220 g (9.3 × 10^{-5} mol) of blue crystals corresponding to the tricationic complex [{Fe(η^5-C_5Me_5)(η^2-dppe)(C≡C)}$_3$(1,3,5-C_6H_3)][PF_6]$_3$ (80% yield). Anal. Calcd for $C_{120}H_{120}F_{18}Fe_3P_9$1/8$CH_2Cl_2$: C, 61.32; H, 5.15. Found: C, 61.11; H, 5.13. FT-IR (Nujol, cm^{-1}): 2012 (νC≡C). Mössbauer (mm/s vs Fe, 77 K): IS 0.25, QS 0.88. UV (CH_2Cl_2): λ_{max} (ϵ/10^3 dm^3 mol^{-1} cm^{-1}) = 288(55.9), 573(5.5), 662(5.5).

Theoretical Calculations. Density functional calculations were carried out on models **1-H**, **2-H**, **3-H**, and **4-H** using the Amsterdam Density Functional (ADF) program[61] developed by Baerends and co-workers[62−65] using nonlocal exchange and correlation corrections.[66] The geometry optimization procedure was based on the method developed by Versluis and Ziegler.[58,59] The atom electronic configurations were described by a double-ζ Slater-type orbital (STO) basis set for H 1s, C 2s and 2p, and P 3s and 3p, augmented with a 3d single-ζ polarization function for the carbon atoms of the bis- or tris-(ethynyl)benzene ligand. A triple-ζ STO basis set was used for Fe 3d and 4s, augmented with a single-ζ 4p polarization function. A frozen-core approximation was used to treat the core electrons of C, P, and Fe. For convenience, calculations on neutral and cationic (**3-H**) models were made using a C_{3v} symmetry instead of a C_{3h} symmetry. Calculations were performed on these models with a lower symmetry (C_s) in order to differentiate the iron centers. They led to comparable results. An extended Hückel[67] fragment analysis was carried out on the DFT-optimized geometries with the program CACAO using standard parameters.[68]

Acknowledgment. We are grateful to Dr. S. Sinbandhit (C.R.M.P.O., Rennes) for NMR assistance. We are also indebted to the Laboratoires Standa (Caen, France) for financial support to T.W. The Centre de Ressources Informatiques (CRI) of Rennes and the Institut de Développement et de Ressources en Informatique Scientifique (IDRIS-CNRS) of Orsay (project 970649) are acknowledged (K.C. and J.-F.H.) for computing facilities.

OM980778H

(57) Parr, R. G.; Yang, W. *Density-Functional Theory of Atoms and Molecules*; Oxford University: New York, 1989.
(58) Ziegler, T. *Can. J. Chem.* **1995**, *73*, 743.
(59) Ziegler, T. *Chem. Rev.* **1991**, *91*, 651−667.
(60) Kohn, W.; Becke, A. D.; Parr, R. G. *J. Phys. Chem.* **1996**, *100*, 12974−12980.
(61) *Amsterdam Density Functional (ADF) Program*, release 2.0.1; Vrije Universteit: Amsterdam, The Netherlands, 1996.
(62) Baerends, E. J.; Ellis, D. E.; Ros, P. *Chem. Phys.* **1973**, *2*, 41−51.
(63) Baerends, E. J.; Ros, P. *Int. J. Quantum Chem.* **1978**, *S12*, 169−190.
(64) Boerrigter, P. M.; Te Velde, G.; Baerends, E. J. *Int. J. Quantum Chem.* **1988**, *33*, 87−113.
(65) Te Velde, G.; Baerends, E. J. *J. Comput. Phys.* **1992**, *99*, 84−98.
(66) Perdew, J. P. *Phys. Rev.* **1986**, *B34*, 7406.
(67) Hoffmann, R. *Chem. Phys.* **1963**, *39*, 1397.
(68) Mealli, C.; Proserpio, D. *J. Chem. Educ.* **1990**, *67*, 399.